ISSN 0001-4338, Izvestiya, Atmospheric and Oceanic Physics, 2018, Vol. 54, No. 5, pp. 446–455. © Pleiades Publishing, Ltd., 2018.
Original Russian Text © B.M. Koprov, V.M. Koprov, O.A. Solenaya, O.G. Chkhetiani, E.A. Shishov, 2018, published in Izvestiya Rossiiskoi Akademii Nauk, Fizika Atmosfery i Okeana, 2018, Vol. 54, No. 5, pp. 525–537.

Technique and Results of Measurements of Turbulent Helicity in a Stratified Surface Layer

B. M. Koprov[a], *, V. M. Koprov[a], O. A. Solenaya[a], O. G. Chkhetiani[a], and E. A. Shishov[a]

[a] *Obukhov Institute of Atmospheric Physics, Russian Academy of Sciences, Moscow, 119017, Russia*

**e-mail: bmkoprov@gmail.com*

Received April 3, 2017; in final form, June 14, 2017

Abstract—In August 2014, measurements of the turbulent velocity rotor, turbulent temperature gradient, turbulent helicity, and turbulent potential vortex were performed at the Obukhov Institute of Atmospheric Physics testing ground in Tsimlyansk under different stratification conditions. The measurements were carried out using the technique first used in the Tsimlyansk expedition in 2012 [1]. The measuring facility consisted of four three-component acoustic Gill Windmaster anemometers–thermometers placed at the vertices of a rectangular tetrahedron with a base scale of 0.7 m (in contrast to the experiment in 2012, when the base scale was 5 m). The measuring facility was placed on top of a mast with an adjustable height of 3.5, 5, 13.5, and 25 m and was equipped with a rotator. The temperature profile in the 10–600 m layer was continuously recorded by the Kadygrov microwave profiler [2]. The series of density of instantaneous helicity $He = u_i'\omega_i' = u_1'\omega_1' + u_2'\omega_2' + u_3'\omega_3'$ and average values of the total and its summands were calculated for 12 daytime and 10 daytime 2-hour intervals. The helicity value averaged over 12 day realizations is about 0.2 m/s^2, and the average cosine is close to 0.08 ± 0.03. At night, the helicity is estimated as 0.07 ± 0.03 m/s^2, and the cosine is close to 0.025 ± 0.03. For the abovementioned 12 daytime and 10 daytime 2-hour intervals, the covariance and correlation matrices of temperature components, velocity rotor, velocity, and temperature gradient are calculated. The off-diagonal terms of the covariance matrix exceed by absolute values the diagonal terms several times. Similar characteristics of a potential vortex were estimated in the incompressibility approximation. The systematic error due to spatial averaging of the measured quantities is discussed.

Keywords: rotor variations, turbulent helicity, turbulent potential vortex

DOI: 10.1134/S0001433818050067

INTRODUCTION

The atmospheric temperature distribution by altitude is generally driven by the heat inflow (or loss) vertical distribution due to longwave radiation [3]. In the surface layer, the radiation heating (or cooling) generates nonequilibrium stratification and initiates turbulent heat transport. In the morning, solar radiation flow heats up the ground surface and increases the intensity of the surface thermal irradiation. This irradiation is most intensively absorbed in the immediate proximity to the surface and creates nonequilibrium stratification. The turbulent mixing smoothes temperature gradients and creates the turbulent heat flow. Therefore, the profile is considered to form outside the roughness layer as a result of the interaction of the radiation and the turbulent flows. The temperature increases parallel to the increasing solar angle. Requirements are close to stationary at the clear sky, when the solar angle and the temperature of the underlying surface are close to their maxima. The altitude variations of the turbulent and the radiation flows are equal by absolute magnitudes and opposite by signs. The radiation heating is set off by turbulent cooling. This is usually observed from 11:00 to 16:00 local solar time. The transformation of the temperature profile in the boundary layer observed during the morning transition period and in the evening in the surface layer of the atmosphere is presented in Figs. 1a and 1b. As follows from Fig. 1b, during the period of transition from instability to stability, the temperature decreases synchronously at all levels, with a simultaneous decrease in the amplitude of its variations. In Fig. 1a referring to the profiler, this feature is less expressed, since the profiler has high inertia. Both curves show that, during most of the day, the stationary state, which is the basic supposition of the semiempirical theory of the Monin–Obukhov ground layer [4], is explicitly disturbed. It is important that, in both cases presented, in the figures, the time interval of steady potential temperature, minimum temperature variations, and maximum rate of mean temperature changes is observed at all altitudes. In this paper we limit our consideration to stationary conditions.

In [5], the temporal variability of instantaneous temperature profiles under stationary conditions was

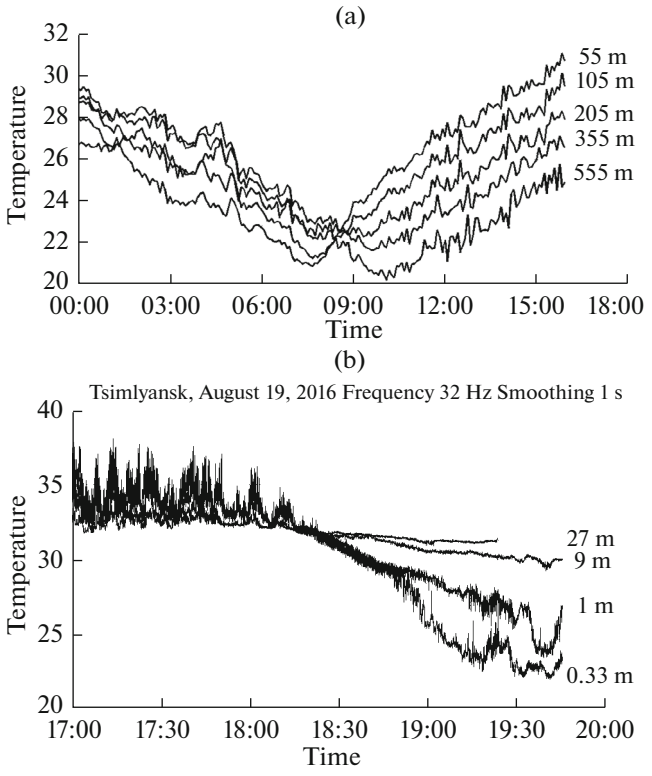

Fig. 1. Example of the temperature dynamics in the morning transition period at altitudes up to 555 m (according to the MTP distant meteorological profiler) (a). Example of the evening temperature dynamics with inversion, according to the readings of five resistance thermometers (b).

explored and the technique of plotting so-called temperature maps, i.e., a time sweep of isothermal surfaces by multipoint low-inertia temperature measurements, was developed. The map presented in Fig. 2 shows that the stratification originating under nonequilibrium conditions with wind does not degrade under stationary conditions, but only isothermal surfaces are deformed. For example, a 33° isotherm changes altitude from 4 to 20 m within 15 s, from 15:20:45 to 15:21:00, and then quickly returns to the initial level. These temperature variations are known as ramp structures [6]. Earlier, in [4], the notion of a coherent structure was introduced as a region with temperatures synchronously exceeding the average level in the range of altitudes of nearly the surface-layer thickness by a value of about its root-mean-square value. These structures are asymmetric; i.e., isothermal surfaces are sparser in their frontal part and denser in their rear part. A supposition was brought forward that the vorticity (velocity rotor) intensified in these regions.

Certainly, this map, based on readings of five thermometers dislocated within the layer of 1.5–24 m, presents a smoothed picture of the instantaneous temperature field. At moderate wind ($v \ll c$, where c is the velocity of sound), when air can be assumed incompressible with an adequate accuracy [7], the density temporal variations within the surface layer are mainly determined by temperature, and, to a lesser degree, by concentrations of water vapor and ozone. Isopicnic surfaces of stratified liquid do not intersect due to the Lagrangian invariance of the density [8]; the isotherms do not intersect either, so the current remains turbulent and maintains the smoothed thermal stratification. As is shown in [5], this statement is valid for both stable and unstable conditions. Thus, the temperature is a kind of tracer, and we can calculate the field of vertical component of the wind velocity using the map of time variations of isotherm altitudes.

The wind field in the bottom part of the surface layer weakly depends on temperature stratification, and the turbulent flow of any impurity is directed towards the concentration decrease. Therefore, for example, in winter, under conditions of steady stratification, when temperature increases with altitude and

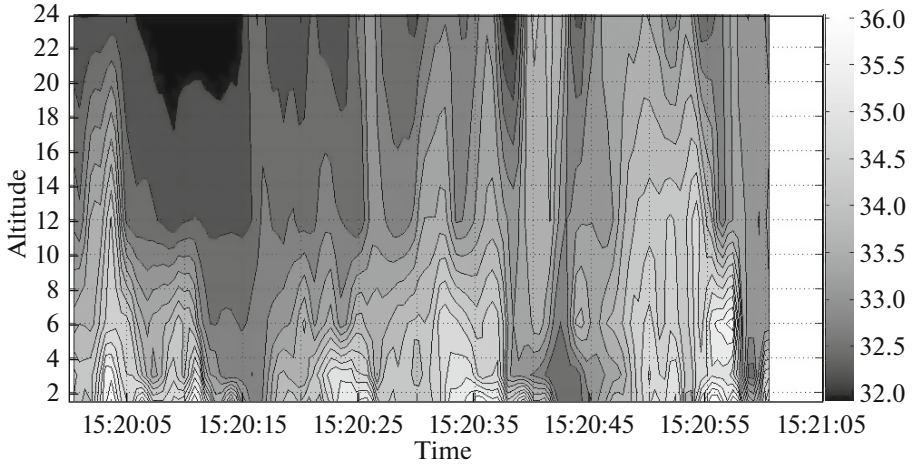

Fig. 2. Example of temperature map under instability conditions.

moisture due to snow evaporation, on the contrary, decreases with altitude, the turbulent heat flow is directed downwards, while the water vapor flow is directed upwards [9].

The scalar product between velocity and rotor, an important scalar describing vortex motions and termed helicity, can be written in the following form:

$$He = u_i\omega_i,$$

where $\boldsymbol{\omega} = \mathrm{rot}\,\mathbf{u}$, and summation is performed over the repeating index from 1 to 3. In this paper we try to find out how great this scalar influence on the turbulent exchange is. This question is being actively explored theoretically. A brief overview of theoretical studies of helicity is presented in [1].

Another important scalar is turbulent potential vortex $\Pi = \overline{\omega_i' (\partial\rho'/\partial x_i)}$, which supposes the following approximate equality to be fair upon an assumption of incompressibility:

$$\Pi \approx (\bar{\rho}/\bar{T})\,\overline{\omega_i' (\partial T'/\partial x_i)},$$

where i means summation from 1 to 3. In the ideal liquid, the potential vortex is an integral of motion [8].

In the large-scale dynamics of the Earth's atmosphere, the helicity of synoptic formations is determined by the Earth's rotation. In the Northern Hemisphere, the helicity of cyclones and anticyclones is positive, i.e., it is independent on the rotation direction. Most (about 80%) mesoscale formations (whirlwinds and tornados) in the Northern Hemisphere have the same sign. This fact allows a supposition that helicity can be observed on a nonrotating planet. As for whirlwinds and vortices of a dust-devil type, they are characterized by upward motion but can have both right and left rotations. Apparently, in this case, the Earth's rotation creates advantage in evolution only for those randomly formed vortices whose helicity sign is positive.

It is known that the vorticity of a liquid element increases with its stretch along the vortex line [10]. Therefore, this effect plays an important role in the formation of localized rotational structures of dust devils; whirlwinds; and types of tornadoes whose velocity and vortex vectors are close to collinear, i.e., $\cos\varphi = \pm 1$.

G. Batchelor in his book presents an example of a steady-state axisymmetric vortex flow [10]. The positional relationships between the velocity and vortex vectors inside spiral vortices are considered to decrease the influence of viscosity on the liquid particle motion. This property is also observed in flows inside pipes in their bends (laminarization). In addition, it is known that blood motion possesses helicity at the aorta outlet.

The knowledge of a sign, mean value, and behavior of temporal variations of the helicity is rather important for studying the turbulent exchange in the surface layer [8]. The Monin–Obukhov semiempirical surface layer theory [4] supposes that the wind altitudinal diversion due to the Coriolis acceleration can be neglected, which allows us to consider the helicity to be zero, so that $\overline{\cos\varphi} = 0$. Here, by helicity we mean the product between the variations of velocity and rotor averaged by time at one point.

For the first time, the matrix of turbulent covariances of velocity and rotor components (vortex flow) under the conditions of surface layer was theoretically studied by E.A. Novikov [11]. The first attempt to experimentally test the conclusions of this paper was undertaken by us in [12]. The phase acoustic approach was applied to measure the rotor components as velocity circulations along a contour 6 cm in size according to the technique proposed by V.M. Bovsheverov [13]. The diagonal elements of covariance matrix $\overline{u_i'\omega_j'}$ were not measured. Note that, contrary to predictions made in [11], not only the nondiagonal terms of matrix $\overline{u_i'\omega_j'}$, but also the terms of another diagonal appeared to be zero: $\overline{u_1'\omega_3'}$, $\overline{u_3'\omega_1'}$. In [12], cospectra of the velocity and rotor components, as well as spectral correlation coefficients, were examined.

D.Yu. Sokolov, guided by Bovsheverov's plan, proposed a construction with a two-component circulation meter with a frame of about 0.5 m in combination with a three-component anemometer. This allowed measuring some elements of the covariance velocity and rotor matrix including the helicity summands [14], as well as estimating some two-point and three-point momenta. These works were carried out in summer at an altitude of 46 m at Zvenigorod station of the Obukhov Institute of Atmospheric Physics. The first measurements of mean helicity in the surface atmospheric layer gave us an estimation of $\overline{\cos\varphi}$ of about a few hundredths. This means that the instantaneous helicity, i.e., the product between velocity and rotor variations, is a random process in which the amplitude of variations is at least an order higher than the mean value.

The first joint measurements of helicity He and potential vortex Π in the surface layer were made in the Tsimlyansk expedition in 2012 and described in [1]. The measuring facility consisted of four ultrasonic anemometers–thermometers placed at the vertexes of the rectangular tetrahedron, i.e., a tetrahedron with all right interedge angles at one of its vortices. The base anemometer was at the rectangular vertex at the altitude of 5 m, and its distance from each of other three vertices was 5 m. Spatial derivatives were substituted for differences divided by distances. It was found that the helicity vertical summand $\overline{u_3'\omega_3'}$ had a positive sign, like the large-scale helicity of cyclones and anticyclones of the Northern Hemisphere. On the contrary, the sum of horizontal summands was negative and

exceeded the verticals by module, so that the total was negative.

The rotor values used upon calculating the velocity and rotor covariances are the mean values of rotor by volume with a typical size of 5 m; the velocity at one of the tetrahedron vertexes (namely, the rectangular vertex) is taken as the velocity. Both factors might render a considerable impact on local values of covariances, in particular, the value of covariance $\overline{u_3'\omega_3'}$. We cannot exclude that the helicity negative sign observed in the experiment of 2012 was determined by this circumstance.

Therefore, in 2014, a new attempt of joint measurements of the helicity and potential vortex using a tetrahedron of considerably smaller size (0.7 m) placed on top of a mast of variable altitude was undertaken. This allowed us to measure the parameters at altitudes of 3.5, 5, 13.5, and 25 m. To explore the relation between the coherent structures and the helicity, we introduced the measuring of the temperature instantaneous profile by the technique developed in [5] into the program. In this paper we have focused on studying helicity.

MEASURING FACILITY

A measuring facility comprising four Gill anemometers placed on a board on top of an Unzha mast at the vertices of a tetrahedron with a base of 0.7 m is shown in Fig. 3. To minimize the aerodynamic noise from the devices installed on the facility frame, the opportunity of alignment along the wind was envisioned: before measuring, the facility was directed so that the bisectrix of the right angle of the tetrahedron horizontal edge was positioned approximately along the wind line. For this purpose, a bearing was placed between the mast top and the frame. Thus, the measuring volume could be moved forward (into the wind) to a distance about 1-m from the basic elements of the frame structure.

The instantaneous temperature profile was measured by five resistance thermometers with an inertia of 0.01 s placed logarithmically uniformly between the surface and the mast top.

The plan of the consequent processing of measurements includes studying the response of the instantaneous temperature profile and the instantaneous helicity to the transit of shadows of cumulus clouds; therefore, a sensor of the incident solar radiation is included into the measuring facility.

DATA RECORD AND PROCESSING

Data were recorded day and night in a series of no less than 2 h with 20 Hz frequency. The majority of records refer to an altitude of 25 m. The total duration of recording over the period from August 4 to 22 exceeded 200 h. Upon finding the wind direction averaged over the series by the readings of a basic

Fig. 3. Mounting the Tetrahedron facility on top of the mast.

anemometer (located at the tetrahedron rectangular vertex), the transition to meteorological coordinates was made, whose x axis was directed along the mean wind direction. In this coordinate system, all necessary parameters were calculated: the series of rotor and velocity vector component variations, temperature, and temperature gradient.

A specialized IfaLab software package with a visual interface created by us was the basic tool of processing the data. This package provides opportunities to find not only the second momenta, which is enough for examining turbulent helicity and potential vortex, but also the flows of these scalars and other third momenta. During an appropriate tuning, some other general functions can be calculated, for example, cross momenta of any order, which enables one to explore relations between helicity and potential vortex, which was considered theoretically in some papers. Using the IfaLab package, we have calculated, in particular, autospectra and cospectra, spectral correlation coefficients, probability distributions, and temperature maps. Special tools are stipulated in the package for obtaining variations by subtracting the moving average by the window of the given size, and the size was usually 20 min.

RESULTS OF MEASUREMENTS

An example of the daytime implementation of helicity is shown in Fig. 4.

For 12 daytime and 10 nighttime 2-h measuring intervals, matrices of correlations–covariations for all pair combinations of the following ten parameters were calculated:

$$T',\ \omega_x',\ \omega_y',\ \omega_z',\ u_x',\ u_y',\ u_z',\ G_x',\ G_y',\ G_z'.$$

In Fig. 5, one of the daytime matrices is displayed and Fig. 6 shows one of the nighttime matrices. Let-

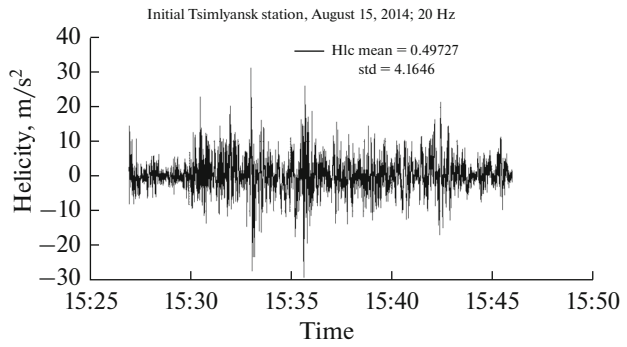

Fig. 4. Helicity over the interval of 20 min.

ters R, V, and G included in the notations of lines and columns correspond to rotor, velocity, and temperature gradient; letters x, y, and z indicate the component direction: downwind, across the wind, or in the vertical direction. For example, Rx is the component of vector R along the x axis, i.e., downwind. The diagonal of the matrix presents dispersions, correlations are placed to the left of the diagonal, and covariances are to the right of the diagonal.

The data on the velocity component covariances and their correlations, like the data on covariations and correlations of the velocity and temperature, agree with the experimental data obtained earlier during long-term research [15]. Covariance $\overline{\omega_z' T'}$ changes its sign from day to night, and the corresponding correlation coefficient $r_{\omega_z T} = \overline{\omega_z' T'} \Big/ \sigma_{\omega_z} \sigma_T$, both during the day and during the night, was insignificant by module in comparison with the coefficient of temperature correlation with the velocity longitudinal and vertical components, as well as with other components of vector $\boldsymbol{\omega}$.

Consolidated data on helicity, potential vortex, and conditions of measuring are presented in Table 1. In Table 2, data on helicity and potential vortex and their summands obtained by processing 12 daytime series are presented and, in Table 3, these parameters for 10 nighttime measurements are given. The mean value of cosφ is positive for both daytime and nighttime implementations and close to 0.08 ± 0.03 and 0.025 ± 0.008, respectively; the helicity was negligibly small and negative only in one daytime and one nighttime series. This means that average angle φ is almost always less than 90°: in the daytime the difference is 4.5°, and in the nighttime it is 1.5°. The fact that the helicity vertical component is positive under conditions of both stable and unstable stratification agrees with the results of 2012 corresponding to the altitude of 5 m.

The modules of diagonal elements of the covariance matrix $\overline{u_i' \varpi_j'}$ are on average several times smaller than other term modules. The same is true with the correlation coefficients. Meanwhile, the maximum values of the nondiagonal correlation coefficient modules exceed 0.5; i.e., they are comparable to the coefficients of correlation between the velocity and temperature components.

*	$T4$	R_x	R_y	R_z	V_x	V_y	V_z	G_x	G_y	G_z
$T4$	0.2946	0.1370	–0.1033	0.0116	–0.3003	–0.1212	0.1554	0.1249	0.2232	–0.1312
R_x	0.1183	4.5526	–0.4107	1.9405	–0.1421	0.9183	0.5337	0.1454	0.4531	–0.1923
R_y	–0.1124	–0.1137	2.8671	1.0271	–0.5727	0.2935	–0.2739	–0.1965	–0.1140	0.0279
R_z	0.0084	0.3570	0.2381	6.4906	–1.2915	1.3252	0.1765	0.0029	0.2374	0.0125
V_x	–0.4225	–0.0509	–0.2583	–0.3872	1.7145	–0.0782	–0.2654	0.0273	–0.1135	–0.0527
V_y	–0.1740	0.3356	0.1351	0.4055	–0.0466	1.6450	0.0540	0.0244	0.0334	–0.0181
V_z	0.4458	0.4624	–0.2519	0.1079	–0.3156	0.0656	0.4125	0.0775	0.1535	–0.0747
G_x	0.3443	0.1020	–0.1737	0.0017	0.0312	0.0285	0.1807	0.4462	0.1903	–0.1864
G_y	0.5263	0.2778	–0.0862	0.1192	–0.1109	0.0333	0.3059	0.3645	0.5186	–0.2217
G_z	–0.3813	–0.1422	0.0260	0.0078	–0.0635	–0.0223	–0.1835	–0.4402	–0.4475	0.4620

Fig. 5. Example of correlation and covariance matrix for an unstable stratification (day): August 15, series 12, trend selection window is 20 min, interval is 14:30–16:13, altitude is 25.1 m.

*	$T4$	R_x	R_y	R_z	V_x	V_y	V_z	G_x	G_y	G_z
$T4$	0.0504	−0.0085	−0.0422	−0.0307	0.0759	0.0011	−0.0167	−0.0495	0.0264	−0.0318
R_x	−0.0453	0.7062	0.1637	−0.2388	0.0045	0.1817	0.0484	0.0244	−0.0507	0.0351
R_y	−0.2082	0.2159	0.8141	0.2546	−0.1707	0.0234	0.1150	0.0951	−0.0770	0.0978
R_z	−0.1256	−0.2607	0.2690	1.1881	−0.1745	−0.2493	0.0289	0.0051	−0.0856	0.0427
V_x	0.5770	0.0092	−0.3229	−0.2734	0.3431	0.0095	−0.0346	−0.0419	0.0255	−0.0187
V_y	0.0100	0.4589	0.0550	−0.4856	0.0344	0.2219	−0.0039	0.0052	−0.0062	0.0031
V_z	−0.3040	0.2347	0.5194	0.1081	−0.2405	−0.0336	0.0602	0.0217	−0.0133	0.0158
G_x	−0.6057	0.0799	0.2893	0.0129	−0.1966	0.0301	0.2428	0.1326	−0.0409	0.0578
G_y	0.3854	−0.1979	−0.2798	−0.2576	0.1430	−0.0434	−0.1779	−0.3679	0.0930	−0.0475
G_z	−0.4490	0.1326	0.3438	0.1243	−0.1011	0.0211	0.2037	0.5037	−0.4938	0.0994

Fig. 6. Example of correlation and covariance matrix for a stable stratification (night): August 11, series 16, trend selection window is 20 min, interval is 23:00–01:00, altitude is 25.1 m.

It is noteworthy that the mean value of helicity vertical component $\overline{u_3'\omega_3'}$ is positive in the majority of the considered daytime and nighttime measurements.

Covariance matrix $\overline{u_i'\omega_j'}$ contains information not only about the series mean helicity, which is the average scalar product between velocity by rotor variations $He = \overline{\mathbf{v}' \cdot \boldsymbol{\omega}'} = \bar{a} \cdot \bar{b} \cdot \cos\varphi$, but also about vector product

$$\overline{\mathbf{A}'} = \overline{\mathbf{v}' \times \boldsymbol{\omega}'} = \mathbf{i}(\overline{v_2'\omega_3'} - \overline{v_3'\omega_2'}) - \mathbf{j}(\overline{v_1'\omega_3'} - \overline{v_3'\omega_1'})$$
$$+ \mathbf{k}(\overline{v_2'\omega_1'} - \overline{v_2'\omega_1'}) = a \cdot b \cdot \sin\varphi,$$

since every summand in brackets included into this expression is an element of the covariance matrix. The examination of correlation–covariation matrices calculated, as mentioned above, for 12 daytime and 10 nighttime measurements (examples are presented in Figs. 5 and 6), shows that the summands in brackets are always of opposite signs, so that the module of every component of vector **A** is the sum of modules of its terms. In this case, the mean turbulent value of sinφ is apparently very close to unit.

At the same time, as was noted above, there are natural localized rotational structures of the dust-devil or tornado types in which the normalized helicity is close to unit and the vector product of velocity by rotor is close to zero. These structures are observed in laboratory experiments with convection above a rotating heated plane [16].

The observed value of turbulent helicity, which is positive at any stratification (and small by absolute value), can be explained by the violation of the bilateral symmetry associated with the wind diversion in cyclones and anticyclones in the Northern Hemisphere, which possess positive helicity. Apparently this is the cause of the preferentially positive sign of helicity in tornados of the Northern Hemisphere. In [17], the importance of taking turbulent helicity into account in models of the atmospheric boundary layer is emphasized.

COSPECTRA OF ROTOR AND VELOCITY COMPONENTS

Seven cospectra of the rotor and velocity components are presented (namely, cospectra: *RxVx*, *RxVy*, *RyVx, RyVy*, *RyVz*, *RzVy*, and *RzVz*) for one of the daytime series in Fig. 7a. Similar cospectra for one of the nighttime series are shown in Fig. 7b. In these figures, real parts of the complex cross-spectral density (cospectra) multiplied by frequency are plotted along the ordinate axis and the frequency logarithm is along the abscissa axis. In this representation, the area under each curve is the integral of the corresponding covariance. Numbers 1, 4, and 7 designate the cospectra, referring to the helicity longitudinal, transverse, and vertical components. Daytime nondiagonal cospectra have maxima near 0.1 Hz and decrease almost to zero at the abscissa deviation in either direction from this value. We can clearly see that, under all conditions, be it day or night, the modules of all diagonal cospectra (responsible for helicity) are several times smaller than any nondiagonal ones. The results of measurements of autospectra and cospectra of the velocity and rotor components are influenced mainly by the spatially

Table 1. Turbulent helicity and turbulent potential vortex

Day/ Night	Date	Series	Altitude	Wind velocity	$\lvert\boldsymbol{\omega}\rvert$	$\lvert\mathbf{u}\rvert$	$\lvert\mathbf{G}\rvert$	H	$\widehat{H}$	P	$\widehat{P}$	ζ
Day												
d	Aug 07 2014	08	3.5	3.1	1.14	0.867	0.236	0.022	0.0217	–0.0012	–0.0043	–0.0343
d	Aug 07 2014	20	13.1	2.3	1.13	0.792	0.505	0.071	0.0796	–0.0071	–0.0124	–0.0783
d	Aug 08 2014	12	25.1	5.9	1.92	2.039	1.070	0.399	0.1021	–0.0069	–0.0033	–18.158
d	Aug 09 2014	12	25.1	2.9	1.55	1.985	0.856	0.499	0.1621	0.0234	0.0176	–4.569
d	Aug 10 2014	12	25.1	3.9	1.49	1.013	0.699	0.135	0.0895	0.0095	0.0091	–3.776
d	Aug 11 2014	08	25.1	3.8	2.21	1.201	1.420	–0.015	–0.0055	0.0362	0.0116	–12.571
d	Aug 12 2014	05	25.1	2.6	2.27	1.465	1.303	0.211	0.0635	0.0663	0.0224	–6.417
d	Aug 15 2014	12	25.1	5.7	3.73	1.942	1.208	0.328	0.0453	0.0440	0.0098	–0.372
d	Aug 18 2014	12	25.1	4.9	2.03	1.164	0.743	0.012	0.0050	0.0015	0.0010	–0.906
d	Aug 19 2014	08	25.1	4.7	1.78	1.961	0.767	0.469	0.1347	0.0137	0.0100	–14.381
d	Aug 21 2014	08	13.1	3.5	1.16	1.031	0.825	0.142	0.1182	0.0256	0.0268	–12.896
d	Aug 22 2014	05	3.5	2.6	2.02	1.107	1.158	0.124	0.0553	0.0539	0.0231	–0.1569
Night												
n	Aug 07 2014	32	25.1	2.7	0.58	0.416	0.299	0.014	0.0558	–0.0035	–0.0200	2.224
n	Aug 08 2014	20	25.1	3.2	0.37	0.254	0.306	0.001	0.0123	0.0001	0.0005	0.0676
n	Aug 09 2014	04	25.1	2.9	0.40	0.382	0.276	0.006	0.0398	–0.0005	–0.0046	–0.149
n	Aug 09 2014	17	25.1	5.4	1.24	0.502	0.596	0.006	0.0089	–0.0026	–0.0036	0.959
n	Aug 10 2014	04	25.1	5.2	0.84	0.368	0.670	0.004	0.0141	0.0009	0.0016	2.0518
n	Aug 11 2014	16	25.1	4.4	1.65	0.791	0.570	0.057	0.0437	–0.0098	–0.0105	1.045
n	Aug 15 2014	04	25.1	3.7	1.21	0.616	0.568	0.054	0.0722	–0.0129	–0.0187	1.176
n	Aug 17 2014	12	25.1	7.1	2.48	1.137	0.438	0.020	0.0072	–0.0022	–0.0020	0.2878
n	Aug 19 2014	12	13.1	3.3	0.89	0.577	0.325	0.021	0.0412	0.0016	0.0057	0.5392
n	Aug 20 2014	08	13.1	1.5	0.16	0.132	0.189	–0.001	–0.0560	–0.0001	–0.0025	13.971

Registration frequency is 20 Hz and window of the trend subtraction is 20 min. $H = (\boldsymbol{\varpi} \cdot \mathbf{u})$, $P = (\boldsymbol{\varpi} \cdot \mathbf{G})$, $\widehat{H} = \dfrac{H}{|\boldsymbol{\varpi}| \cdot |\mathbf{u}|}$, $\widehat{P} = \dfrac{P}{|\boldsymbol{\varpi}| \cdot |\mathbf{G}|}$, $\varsigma = \dfrac{z}{L}$, and L is the Obukhov scale.

Table 2. Turbulent helicity and turbulent potential vortex under instability conditions (daytime series)

Date	Series	Altitude	Wind velocity	Start	Finish	Helicity				Potential vortex			
						H	covariations			P	covariations		
							R_x, V_x	R_y, V_y	R_z, V_z		G_x, V_x	G_y, V_y	G_z, V_z
07	08	3.5	3.1	10:35	11:34	0.0216	0.0321	–0.0021	–0.0084	–0.0011	–0.0020	–0.0015	0.0023
07	20	13.1	2.3	15:30	17:11	0.0712	0.0313	0.0154	0.0245	–0.0071	–0.0048	–0.0011	–0.0012
08	12	25.1	5.8	11:30	13:30	0.4623	0.2370	0.2105	0.0148	–0.0013	–0.0001	0.0218	–0.0230
09	12	25.1	2.8	11:47	13:10	0.6170	0.1995	0.3621	0.0555	0.0300	0.0089	0.0109	0.0102
10	12	25.1	3.9	16:03	18:00	0.1354	0.0157	0.1285	–0.0087	0.0095	0.0106	0.0031	–0.0041
11	08	25.1	3.8	11:30	14:30	–0.0120	–0.0128	0.0344	–0.0335	0.0345	0.1581	–0.0804	–0.0432
12	05	25.1	2.6	13:30	16:00	0.2114	0.1079	0.1429	–0.0394	0.0665	0.0029	0.0436	0.0201
15	12	25.1	5.7	14:30	16:30	0.3277	–0.1422	0.2933	0.1766	0.0440	0.1455	–0.1141	0.0126
18	12	25.1	4.9	15:06	17:15	0.0118	0.0393	–0.0266	–0.0009	0.0015	0.0271	–0.0203	–0.0054
19	08	25.1	4.5	15:46	16:56	0.4641	0.2313	0.2142	0.0186	0.0248	–0.0188	0.0340	0.0095
21	08	13.1	3.5	13:06	14:00	0.1415	0.0499	0.0920	–0.0004	0.0257	0.0191	–0.0043	0.0109
22	05	3.5	2.6	08:30	10:30	0.1235	–0.0038	0.0571	0.0702	0.0541	0.0896	–0.0181	–0.0175
Average over daytime series						0.2146	0.0654	0.1268	0.0224	0.0234	0.0363	–0.0105	–0.0024

Registration frequency is 20 Hz and window of the trend subtraction is 20 min.

averaged data from velocity and rotor sensors and their positional relationship, which is described by the spectral transfer factor. Its calculations are very difficult even for the rotor autospectrum, and the more so for cospectra $u_i'\omega_j'$. We tried to estimate the influence of the instrumental averaging by a comparison of cospectra measured using sensors with a considerable size difference (about 0.7 m in the measurements of 2014 and 6 cm in the studies of 1994 [9]). A tentative conclusion is that the integral value of covariances in the experiments of 2014 can be underestimated by about 40% due to the instrumental averaging.

In Fig. 8, the relation between the normalized helicity and parameter ς is shown.

COSPECTRA OF COMPONENTS OF THE ROTOR AND THE TEMPERATURE GRADIENT

The concept of potential vortex was introduced into the atmospheric dynamics by Rossby, Erthel and Obukhov independently. This term reflects the fact that the liquid density inhomogeneity can be a source of a flow vorticity [6].

The value of cosφ for a potential vortex averaged over the total data set was +0.0065 in the daytime and −0.0039 in the nighttime, so that the angle between vectors **v** and **G** deviated from 90° by only tenths of a degree on average.

In Figs. 9a and 9b, seven cospectra of the rotor and the temperature gradient components (namely cospectra *RxGx*, *RxGy*, *RyGx*, *RyGy*, *RyGz*, *RzGy*, and *RzGz*) are shown for one daytime and one nighttime implementations, in which cosφ is close to the mentioned mean values. Unlike cospectra of helicity components, i.e., of elements of the principal diagonal of covariance matrix $u_i\omega_j$, the diagonal cospectra of the potential vortex are not always small when compared with all others. In addition, the figure shows that diagonal cospectra R_yG_y, R_zG_z have close to similar ampli-

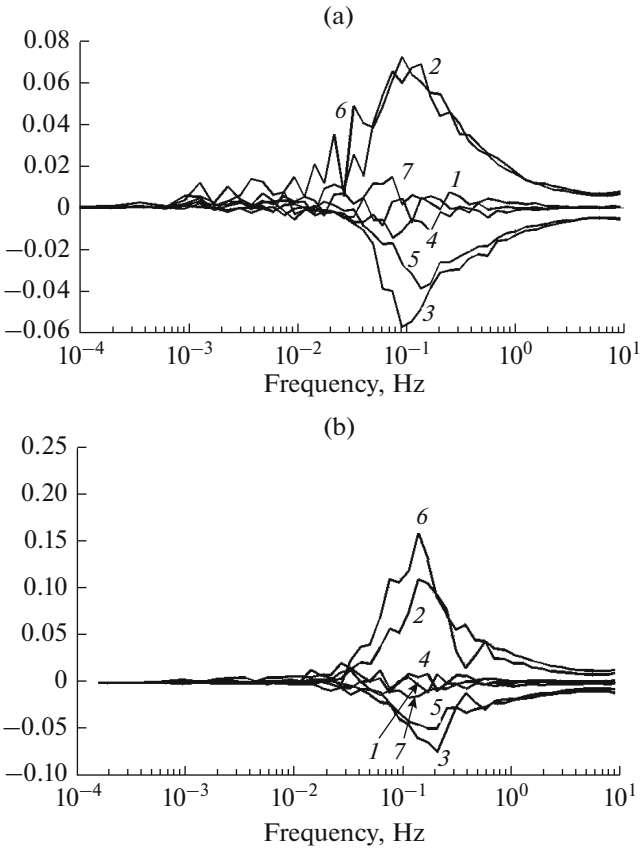

Fig. 7. (a) Examples of rotor and velocity cospectra under instability conditions: (*1*) *RxVx*, (*2*) *RxVy*, (*3*) *RyVx*, (*4*) *RyVy*, (*5*) *RyVz*, (*6*) *RzVy*, and (*7*) *RzVz*. (b) Example of rotor and velocity cospectra under stability conditions: (*1*) *RxVx*, (*2*) *RxVy*, (*3*) *RyVx*, (*4*) *RyVy*, (*5*) *RyVz*, (*6*) *RzVy*, and (*7*) *RzVz*.

Table 3. Turbulent helicity and turbulent potential vortex under stability conditions (night series)

Date	Series	Altitude	Wind velocity	Start	Finish	Helicity				Potential vortex			
						H	covariations			P	covariations		
							R_x,V_x	R_y,V_y	R_z,V_z		G_x,V_x	G_y,V_y	G_z,V_z
07	32	25.1	2.7	22:59	01:01	0.0135	0.0138	0.0047	−0.0049	−0.0035	0.0006	0.0000	−0.0041
08	20	25.1	3.2	21:36	23:36	0.0011	0.0027	−0.0034	0.0019	0.0001	−0.0003	0.0065	−0.0061
09	04	25.1	2.9	02:00	04:00	0.0059	0.0062	0.0019	−0.0023	−0.0004	0.0002	0.0051	−0.0057
09	17	25.1	5.4	22:15	00:15	0.0055	0.0495	−0.0047	−0.0393	−0.0026	0.0254	0.0372	−0.0652
10	04	25.1	5.2	02:30	04:30	0.0067	0.0135	0.0081	−0.0149	0.0039	0.0243	0.0350	−0.0553
11	16	25.1	4.6	00:00	02:00	0.0444	0.0098	0.0116	0.0230	−0.0149	0.0324	−0.0855	0.0381
15	04	25.1	3.7	02:00	04:00	0.0539	−0.0175	0.0451	0.0263	−0.0129	−0.0304	−0.0349	0.0524
17	12	25.1	7,1	23:59	02:00	0.0201	0.0456	0.0475	−0.0730	−0.0021	−0.0096	0.0490	−0.0415
19	12	13.1	3.3	23:08	01:08	0.0211	0.0205	0.0075	−0.0069	0.0017	0.0008	0.0193	−0.0185
20	08	13.1	1.5	20:30	22:30	−0.0012	0.0000	−0.0015	0.0002	−0.0001	0.0002	0.0001	−0.0004
Average on nighttime series						0.0171	0.0144	0.0117	−0.009	−0.0031	0.0044	0.0032	−0.0106

Registration frequency is 20 Hz and window of the trend subtraction is 20 min.

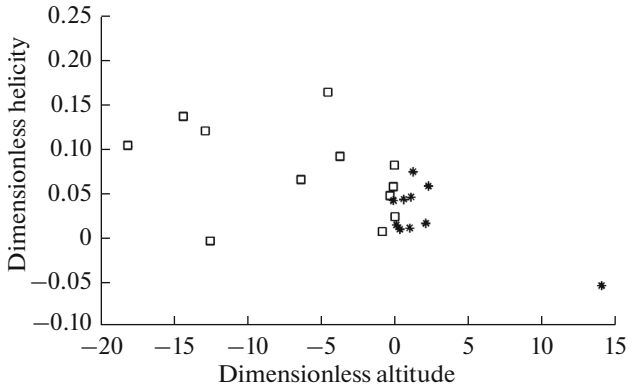

Fig. 8. Dimensionless helicity $\cos\varphi$ as a function of dimensionless altitude $\varsigma = z/L$.

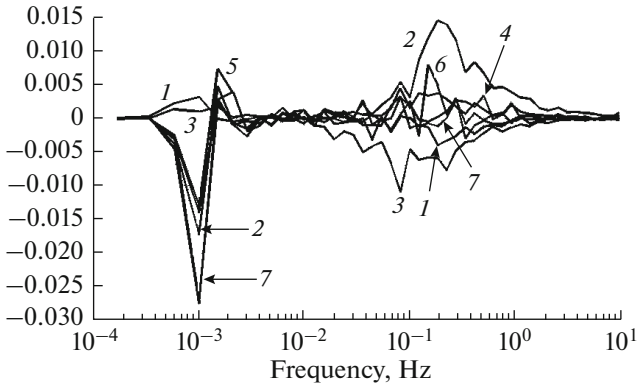

Fig. 10. Example of rotor and temperature gradient cospectra under instability conditions. The case with additional extrema: (*1*) *RxGx*, (*2*) *RxGy*, (*3*) *RyGx*, (*4*) *RyGy*, (*5*) *RyGz*, (*6*) *RzGy*, and (7) *zGz*.

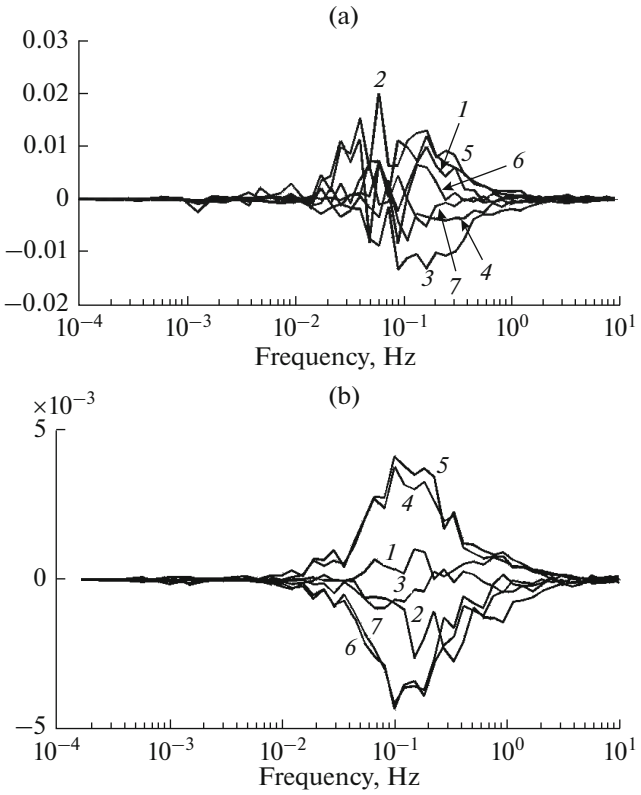

Fig. 9. (a) Example of rotor and temperature gradient cospectra under instability conditions: (*1*) *RxGx*, (*2*) *RxGy*, (*3*) *RyGx*, (*4*) *RyGy*, (*5*) *RyGz*, (*6*) *RzGy*, and (*7*) *RzGz*. (b) Example of rotor and temperature gradient cospectra under stability conditions: (*1*) *RxGx*, (*2*) *RxGy*, (*3*) *RyGx*, (*4*) *RyGy*, (*5*) *RyGz*, (*6*) *RzGy*, and (*7*) *RzGz*.

tudes and opposite signs, so that they cancel each other, while the amplitude of cospectrum R_xG_x is small in comparison with them.

Some cospectra of rotor and temperature gradient components display the second low-frequency extremum (in this case, negative) at a frequency of about 10^{-3} Hz, which makes a considerable contribution to the respective covariance (Fig. 10). Note that the filter corresponding to a subtraction of a 20-min moving average cuts off variations with frequencies below 1.4×10^{-4} Hz, but hardly influence the variation with the frequency of 10^{-3} Hz. Apparently spectral analysis allows separating the wave and the turbulent contributions to helicity.

The low-frequency maximum is observed in the cases of quasiperiodic large-amplitude variation trains with the frequency of about 10^{-3} Hz in implementations of the velocity longitudinal components. This is true, in particular, for the implementation recorded from 11:38 to 13:38 on August 20 (Fig. 11). These variations were repeatedly recorded earlier under similar conditions. They might be generated by gravity waves emitted by atmospheric fronts and orographic disturbances in the steady-state stratified atmosphere.

MAIN RESULTS

(1) The procedure of measuring the rotor, temperature gradient, helicity, and potential vortex in regards to the turbulent component of air motions in the near surface layer is developed. This procedure is based on a four-point measurement of velocities and acoustic temperature using four acoustic anemometers, and the subsequent calculation of all necessary parameters using specially created software. The performed measurements are of ordinary duration, of about 200 h, the registration frequency is 20 Hz, and altitudes vary from 3.5 to 25 m.

(2) For 12 day and 10 night 2-h measurement intervals, the expanded archive storages are created, in which, alongside primary series (velocities and temperatures from four anemometers), the calculated series of turbulent rotor, temperature gradient, helicity, and potential vortex are recorded.

(3) For the abovementioned 12 day and 10 night 2-h measurement intervals, the matrices of correlation–

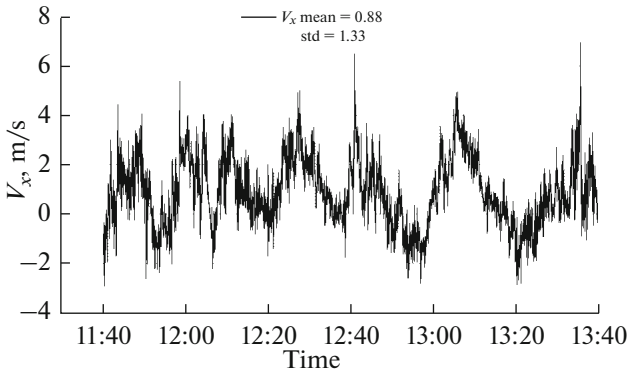

Fig. 11. Quasiperiodic wind variations in the realization for which the cospectrum shown in Fig. 10 is calculated.

covariation of the following ten parameters are calculated: T', ω_x', ω_y', ω_z', u_x', u_y', u_z', G_x', G_y', G_z'.

(4) The average helicity is estimated to be 0.2 m/s^2, the mean cosine is 0.08 ± 0.03 during the day, and the mean cosine is close to 0.025 at nighttime, while the helicity is close to (0.07 ± 0.03) m/s^2.

(5) Cospectra of variations of the rotor and velocity components are obtained.

(6) Cospectra of variations of the rotor and temperature-gradient components are obtained.

(7) The systematic error (underestimation) of integral values of covariations between the velocity and rotor components due to the spatial averaging is estimated.

(8) The dependence of the dimensionless helicity on the dimensionless altitude is obtained.

ACKNOWLEDGMENTS

We are grateful to M.V. Kurganskii for useful discussions. This study was supported by the Russian Science Foundation, project no. 14-27-00134.

REFERENCES

1. B. M. Koprov, V. M. Koprov, M. V. Kurgansky, and O. G. Chkhetiani, "Helicity and potential vorticity in surface turbulence," Izv., Atmos. Ocean. Phys. **51** (6), 565–575 (2015).
2. E. N. Kadygrov and I. N. Kuznetsova, *Methodical Recommendations on the Use of Data on Temperature Profiles in the Atmospheric Boundary Layer Measured Remotely by Microwave Profilometers: Theory and Practice* (Fizmatlitkniga, Dolgoprudnyi, 2015) [in Russia].
3. A. A. Fridman, "O raspredelenii temperatury s vysotoi pri nalichnosti luchistogo teploobmena Zemli i Solntsa," Izv. Gl. Astron. Obs., No. 2, 42 (1920).
4. A. S. Monin and A. M. Obukhov, "Main regularities of turbulent mixing in the atmospheric surface layer," Tr. Inst. Geofiz. Akad. Nauk SSSR **24**, 163–187 (1954).
5. B. M. Koprov, V. M. Koprov, and T. I. Makarova, "Convective structures in the atmospheric surface layer," Izv., Atmos. Ocean. Phys. **36** (1), 37–47 (2000).
6. R. A. Antonia, A. J. Chambers, C. A. Friehe, and C. W. Van-Atta, "Temperature ramps in the atmospheric surface layer," J. Atmos. Sci. **36** (1), 99–108.
7. L. D. Landau and E. M. Lifshits, *Hydrodynamics* (Nauka, Moscow, 1986) [in Russian].
8. F. V. Dolzhansky, *Basics of Geophysical Hydrodynamics* (Fizmatlit, Moscow, 2011) [in Russian].
9. L. G. Elagina, B. M. Koprov, and D. F. Timanovskii, "Some characteristics of the atmospheric surface layer over snow," Izv. Akad. Nauk, Fiz. Atmos. Okeana **14** (9), 926–931 (1978).
10. G. Batchelor, *An Introduction to Fluid Dynamics* (Cambridge University Press, Cambridge, 1967; Mir, Moscow, 1973)
11. E. A. Novikov, "Vortex flow," Izv. Akad. Nauk SSSR, Fiz. Atmos. Okeana **8** (7), 459–462 (1972).
12. B. M. Koprov, V. V. Kalugin, and N. S. Thieme, "Turbulent flow of a vortex," Izv. Akad. Nauk, Fiz. Atmos. Okeana **30** (1), 13–17 (1994).
13. V. M. Bovsheverov, A. S. Gurvich, A. M. Kochetkov, and S. O. Lomadze, "Measurement of the frequency spectrum of small-scale circulation of velocity," Izv. Akad. Nauk, Fiz. Atmos. Okeana **7** (4), 371–376 (1971).
14. B. M. Koprov, V. M. Koprov, V. M. Ponomarev, and O. G. Chkhetiani, "Experimental studies of turbulent helicity and its spectrum in the atmospheric boundary layer," Dokl. Phys. **50** (8), 419–422 (2005).
15. J. C. Kaimal, J. C. Wyngaard, and Y. Izumi, "Spectral characteristics of surface-layer turbulence," Q. J. R. Meteorol. Sci. **98**, 563–589 (1972).
16. B. M. Boubnov and G. S. Golitsyn, *Convection in Rotating Fluids* (Kluwer, Dordrecht, 1995).
17. A. V. Belyan, S. S. Moiseev, and O. G. Chkhetiani, "On turbulent viscosity in helical turbulence," Dokl. Akad. Nauk **334** (1), 34–36 (1994).

Translated by N. Semenova